INSTITUTE OF PHYSICS PUBLISHING PLASMA PHYSICS AND CONTROLLED FUSION

Plasma Phys. Control. Fusion **45** (2003) 43–52 PII: S0741-3335(03)36239-6

Study of neoclassical transport properties of W7-X using the integration along magnetic field lines

V V Nemov[1], S V Kasilov[1], C Nührenberg[2], J Nührenberg[2], W Kernbichler[3] and M F Heyn[3]

[1] Institute of Plasma Physics, National Science Center 'Kharkov Institute of Physics and Technology', Akademicheskaya str. 1, 61108 Kharkov, Ukraine
[2] Max-Planck-Institut für Plasmaphysik, Teilinstitut Greifswald IPP-EURATOM Association, D-17491 Greifswald, Germany
[3] Institut für Theoretische Physik, Technische Universität Graz, Petersgasse 16, A-8010 Graz, Austria

Received 26 April 2002
Published 6 December 2002
Online at stacks.iop.org/PPCF/45/43

Abstract

Using methods based on an integration along magnetic field lines in a given magnetic field, the $1/\nu$ neoclassical transport as well as the variation of the second adiabatic invariant on a magnetic surface are studied for the Wendelstein 7-X (W7-X) standard high-mirror configuration. The analysed quantities are calculated for the magnetic field presented in magnetic coordinates as well as for the vacuum magnetic field. The results obtained for large numbers of magnetic field harmonics are compared to results with a truncated set of harmonics.

1. Introduction

It is well known that one of the principal advantages of stellarators is that they do not require the generation of a toroidal current to confine a plasma and that in contrast to tokamaks they can easily be operated in steady state. However, with respect to a number of confinement parameters stellarators have to be improved. In particular, for the classical standard stellarator, the level of neoclassical transport is unacceptably high. Therefore, at present many stellarator optimization studies are performed worldwide.

In this paper, neoclassical transport properties of Wendelstein 7-X (W7-X) [1, 2] which is an optimized stellarator of the Helias-type [3] are re-discussed. These properties have been already studied in the design phase of this device with either the DKES code or with a Monte-Carlo technique (see, e.g. [2]). In particular, an effective ripple of about 1.5% and an improved confinement of trapped particles have been found in these studies. Some of these points are analysed here using new methods based on the integration along magnetic field lines in a given magnetic field. The magnetic field for the standard high-mirror variant of W7-X is represented in the form of spectra in Boozer magnetic coordinates [4]. Two versions of

the field which correspond to vanishing beta and to finite beta of 4.8% are considered. Some of the calculations are made also for the vacuum magnetic field represented in real-space coordinates.

For an effective ripple evaluation, the technique of the $1/\nu$ transport calculation which was derived in [5] is used. To analyse the sensitivity of the obtained results to the number of harmonics in the Boozer spectrum, computations are performed for various data sets which characterize the magnetic field. Sets which contain excessively large numbers of harmonics (complete data sets, 825 harmonics for every function) as well as sets truncated to the ten or hundred largest harmonics are considered.

For the zero beta case, calculations in real-space coordinates are also performed. The corresponding vacuum magnetic field is presented as a superposition of a finite number of toroidal harmonic functions. For the finite beta case, in addition to the effective ripple the variation of the second adiabatic invariant J on a magnetic surface is also studied. This quantity characterizes the bounce-averaged drift across magnetic surfaces for orbits of locally trapped particles and it is calculated with the method proposed in [6].

The paper is arranged as follows. In section 2 the link between the effective ripple and the $1/\nu$ neoclassical transport is discussed. The computational results for the effective ripple are presented in section 3. The variation of J on a magnetic surface is studied in section 4. Finally, a discussion of all results is given in section 5.

2. Effective ripple and $1/\nu$ neoclassical transport

An effective ripple, $\epsilon_{\rm eff}$, obtained from neoclassical transport computations in the $1/\nu$ regime is often used for evaluating the confinement properties of stellarator systems. For an arbitrary stellarator magnetic field, the particle flux density F_n in this regime can be presented as [5]

$$F_n = -\frac{\sqrt{8}}{9\pi^{3/2}}\frac{v_{\rm T}^2\rho_{\rm L}^2}{\nu R^2}\epsilon_{\rm eff}^{3/2}\int_0^\infty \frac{{\rm d}z\,{\rm e}^{-z}z^{5/2}}{A(z)}\frac{n}{f_{\rm M}}\frac{\partial f_{\rm M}}{\partial r}. \tag{1}$$

Here, $f_{\rm M} = f_{\rm M}(\psi, w)$ is the Maxwellian distribution as a function of the particle energy w and the magnetic surfaces label ψ, $v_{\rm T} = \sqrt{2T/m}$ is the thermal velocity, $\rho_{\rm L} = mcv_{\rm T}/(eB_0)$ is the mean Larmor radius, B_0 is a reference magnetic field, νA is a pitch-angle scattering frequency [7], R is the major radius of the torus. The integral over z in (1) corresponds to the integration over the particle energy w. An equivalent equation for the energy flux density differs from (1) by the factor zT in the sub-integrand. So, the characteristic features of the specific magnetic field geometry manifest themselves through the factor $\epsilon_{\rm eff}^{3/2}$. The result (1) differs from the corresponding formula for the classical stellarator model [7] (standard stellarator) by a simple replacement of the helical modulation amplitude along the magnetic field line, $\epsilon_{\rm h}$, with the quantity $\epsilon_{\rm eff}$. Note that $A(z)$ is a quantity related to the collision operator (see, e.g. [7]). Together with the Coulomb collision frequency, ν, it can be presented in the following form (j and k are indices for different types of particles):

$$\nu_j = \frac{4\sqrt{2\pi}\lambda e^4 n}{3\sqrt{m_j}T_j^{3/2}}, \qquad A_j = \sum_k \frac{3\sqrt{\pi}}{8}\left[\mu_k\left(1-\frac{1}{2z_k}\right)+\mu_k'\right]z_j^{-3/2},$$

$$\mu_j \equiv \mu(z_j) = \frac{2}{\sqrt{\pi}}\int_0^{z_j}{\rm e}^{-t}\sqrt{t}\,{\rm d}t, \qquad \mu_j' = \frac{{\rm d}\mu_j}{{\rm d}z_j}, \qquad z_j = \frac{m_j v^2}{2T_j}.$$

In accordance with [5], the quantity $\epsilon_{\rm eff}^{3/2}$ is presented as

$$\epsilon_{\rm eff}^{3/2} = \frac{\pi R^2}{8\sqrt{2}} \lim_{L_s\to\infty} \left(\int_0^{L_s} \frac{{\rm d}s}{B}\right) \left(\int_0^{L_s} \frac{{\rm d}s}{B}|\nabla\psi|\right)^{-2} \int_{B_{\rm min}^{\rm (abs)}/B_0}^{B_{\rm max}^{\rm (abs)}/B_0} {\rm d}b' \sum_{j=1}^{j_{\rm max}} \frac{\hat{H}_j^2}{\hat{I}_j},$$

$$\hat{H}_j = \frac{1}{b'} \int_{s_j^{\rm (min)}}^{s_j^{\rm (max)}} \frac{{\rm d}s}{B} \sqrt{b' - \frac{B}{B_0}} \left(4\frac{B_0}{B} - \frac{1}{b'}\right) |\nabla\psi| k_{\rm G}, \qquad \hat{I}_j = \int_{s_j^{\rm (min)}}^{s_j^{\rm (max)}} \frac{{\rm d}s}{B} \sqrt{1 - \frac{B}{B_0 b'}}.$$

This quantity is calculated by integration over the magnetic field line length, s, over the sufficiently large interval 0–L_s, and by integration over the perpendicular adiabatic invariant of trapped particles, $J_\perp$. Such an integration takes into account particles being trapped within one magnetic field ripple as well as particles being trapped within several magnetic field ripples. An essential role in such a calculation belongs to the computation of the geodesic curvature of the magnetic field line, which is given as $k_{\rm G} = (\boldsymbol{h} \times (\boldsymbol{h}\cdot\nabla)\boldsymbol{h}) \cdot \nabla\psi/|\nabla\psi|$ with the unit vector $\boldsymbol{h} = \boldsymbol{B}/B$.

Note that in (1) the derivative of $f_{\rm M}$ is taken with respect to a formal radius of the magnetic surface, r, which corresponds to the definition $(\partial/\partial r) \equiv \langle|\nabla\psi|\rangle(\partial/\partial\psi)$ with

$$\langle|\nabla\psi|\rangle = \lim_{L_s\to\infty} \left(\int_0^{L_s} \frac{{\rm d}s}{B}\right)^{-1} \int_0^{L_s} \frac{{\rm d}s}{B}|\nabla\psi|. \tag{2}$$

It follows from [5] that for calculations in Boozer magnetic coordinates the effective ripple turns out to depend on the spectrum of B and on the average value of $|\nabla\psi|$ with $2\pi\psi$ being the toroidal flux Φ. In this case, the flux and current functions are also necessary. For the calculations in real-space coordinates ψ is a convenient magnetic surface label and the $\nabla\psi$ quantity can be calculated using the method presented in [8].

3. Computational results for the effective ripple

In this section, results of effective ripple computations for the standard high-mirror variant of W7-X are presented. The data sets that are necessary for the effective ripple computation were prepared using the finite beta equilibrium codes VMEC and JMC. Together with flux and current functions, these sets contain spectra of B and $|\nabla s|^2$ with s being the normalized flux label, $s = \Phi/\Phi(1)$, where $\Phi(1)$ corresponds to the boundary surface. With the use of $|\nabla s|$ the $|\nabla\psi|$ value can be easily calculated from

$$|\nabla\psi| = \frac{\Phi(1)}{2\pi}|\nabla s|. \tag{3}$$

Cases with vanishing beta and with finite beta of 4.8% are considered. For every case, calculations are performed for the complete data set (of 825 harmonics for every quantity) as well as for the sets truncated to the ten and hundred largest harmonics on the boundary surface. The radial dependences are determined on a set of discrete radial mesh points $s_j = (j-0.5)/48$, $j = 1, 2, \ldots, 48$. Figure 1 shows cross-sections of the boundary magnetic surface s=1.

Computations are also performed for the case of a vacuum magnetic field presented as a superposition of a finite number of toroidal harmonic functions containing the associated Legendre functions (480 harmonics). In this case, the decomposition coefficients were found using the boundary surface ($s = 1$) equation. The results corresponding to this case are compared to results obtained in magnetic coordinates for vanishing beta. Note that near the boundary of the configuration under consideration the rotational transform ι passes through unity for the case of zero beta. Therefore, in the case of the vacuum field computations, island magnetic surfaces corresponding to $\iota = 1$ near the boundary are present.

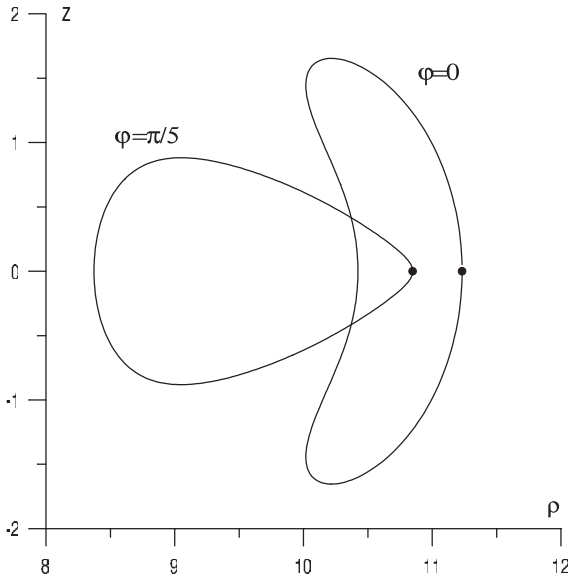

Figure 1. Cross-sections of the boundary magnetic surface. The dots correspond to $\theta = 0$.

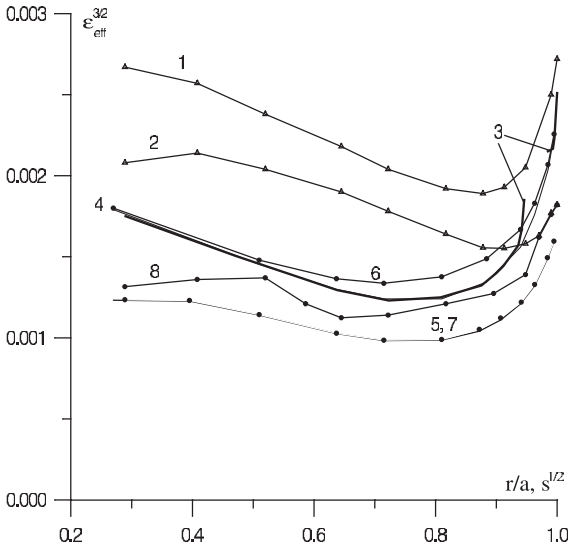

Figure 2. Parameter $\epsilon_{\rm eff}^{3/2}$ for various data sets; 1: zero beta, ten largest harmonics; 2: finite beta, ten largest harmonics; 3: vacuum magnetic field, 480 harmonics (——); 4: zero beta, 825 harmonics (for almost all intervals this curve practically coincides with curve 3, which has a small gap corresponding to islands $\iota = 1$); 5: finite beta, 825 harmonics; 6: zero beta, 100 largest harmonics; 7: finite beta, 100 largest harmonics (practically coincides with curve 5); 8: finite beta, ten largest harmonics selected for every magnetic surface.

The results of $\epsilon_{\rm eff}^{3/2}$ computations are presented in figure 2 as functions of $\sqrt{s}$ (for the computation in magnetic coordinates) or as a function of the normalized mean magnetic surface radius, r/a (for the computation in real-space coordinates, where a is the boundary surface radius). For the magnetic field of the standard stellarator with equivalent sizes the $\epsilon_{\rm eff}^{3/2}$

value turns out to be 0.01–0.03. From figure 2 it follows that the biggest $\epsilon_{\rm eff}^{3/2}$ values obtained in our calculations are approximately one order of magnitude smaller than those for the standard stellarator. The $\epsilon_{\rm eff}^{3/2}$ values for the finite beta case are smaller than those for the case with vanishing beta. These facts are in good agreement with [2].

Figure 2 also shows that the sets with the ten largest harmonics selected at the boundary surface are insufficient for correct computations. The curves 1 and 2 representing the results obtained in this case are essentially higher than the corresponding curves 4 and 5 obtained for the complete data sets. For the case of the hundred largest harmonics (curves 6 and 7) the difference of the results from the corresponding results for the complete data sets is essentially smaller. The curve 6 (zero beta) is only slightly higher than the curve 4. The curve 7 (finite beta) almost coincides with the curve 5.

The difference in the results essentially decreases when the selection of largest harmonics is performed separately for every magnetic surface under consideration. The curve 8 in figure 2 gives an example of the computation results obtained for finite beta in the case of the ten largest harmonics, which were selected separately for every magnetic surface. This curve is much closer to the curve 5 than the curve 2 (for the ten largest harmonics selected for the boundary surface). The behaviour of the curve 8 is less smooth than those for the curves 2 and 5 since every point of the curve 8 corresponds to different harmonic contents in the sets.

From the results it also follows that for the case of vanishing beta the results corresponding to the complete data sets are in good agreement with the results obtained for the vacuum magnetic field in real-space coordinates (bold curve 3 in figure 2). Curves 3 and 4 are very close in figure 2 almost for all values of $\sqrt{s}$ and r/a. Only for a small interval in r/a near the boundary, the curve 3 has a gap corresponding to magnetic islands for $\iota = 1$. For this curve there is a certain increase in $\epsilon_{\rm eff}^{3/2}$ in the vicinity of the islands. Note that inside the islands $\epsilon_{\rm eff}^{3/2}$ changes from 1.3×10^{-3} near the island magnetic axis to $\approx 3 \times 10^{-3}$ near the island boundary surface.

So, the results show that the computational results corresponding to the complete data sets are the results which are numerically best converged; however, for practice-oriented computations, sets truncated to hundred harmonics can be used.

In [2] the value of $\epsilon_{\rm eff} = 1.5\%$ has been reported from MC computations of transport in W7-X. This stays in good agreement with the results presented here. Furthermore, note that the results of the field line integration technique have been successfully benchmarked against MC methods in [5, 9] and also against DKES results in [10].

The large number of harmonics in the full representation of the field (825 harmonics) does not introduce any noticeable error in the results due to finite computer accuracy. Usually, computations of the effective ripple are performed with double precision accuracy in a FORTRAN code. These results stay almost unchanged if, instead, only single precision accuracy is used for the input data. With this reduction of accuracy, the change in results only appears in the seventh decimal digit.

4. Variation of J on a magnetic surface

The trapped particle motion can be described in terms of the second adiabatic invariant $J = \oint v_\parallel \, {\rm d}l$. It is well known that the variation of J on a magnetic surface is closely connected to the bounce-averaged drift of trapped particles across the magnetic surface. Here, this variation is studied for the case of finite beta using the complete data sets. The method derived in [6] is used for this purpose.

The variation of J on a magnetic surface is characterized by the derivative $\partial J/\partial\theta_0$ where $\theta_0 = \theta - \iota\varphi$ with θ and φ being the Boozer angle-like magnetic coordinates and ι being the rotational transform in units of 2π. In accordance with [6], the computational results for

$\partial J/\partial\theta_0$ are presented in a normalized form as a functional dependence between dimensionless parameters η and γ with

$$\eta = \frac{R}{J_\perp}\frac{1}{\tau_b\langle|\nabla\psi|\rangle}\frac{\partial J}{\partial\theta_0}, \qquad \frac{\partial J}{\partial\theta_0} = \frac{e}{mc}\delta\psi, \tag{4}$$

$$\gamma = \frac{v_{\|i}}{v_{\perp 0}}. \tag{5}$$

Here $J_\perp = v_\perp^2/B$, τ_b is the bounce time, $\delta\psi$ is the differential of ψ during τ_b, $v_{\perp 0} = \sqrt{J_\perp B_0}$, $\langle|\nabla\psi|\rangle$ is defined by (2). The $v_{\|i}$ quantity is the parallel velocity $v_\|$ at the point of a local minimum of B for which the $\partial J/\partial\theta_0$ quantity is calculated. The γ parameter is related to the pitch angle at the point of the local minimum of B or, accordingly, to the depth of particle trapping. The normalization of η is performed in such a way that for the standard stellarator magnetic field [7], the result is $\eta = \eta_m \sin\vartheta$ where ϑ is the poloidal angle in quasi-toroidal coordinates and η_m=0.5.

First, computational results for the outer magnetic surface corresponding to $s = s_{48} = 0.989\,583\,3$ are given. Figure 3 shows the values of $b = B/B_0$ along the magnetic field line over the range of 85 local minima of B. Every fifth of the local minima of B is marked by the corresponding number. A number of characteristic results for $\partial J/\partial\theta_0$ expressed through η as functions of γ are presented in figures 4–6. The curves are numbered in accordance with the numbering of the minima of B in figure 3. These curves show η values for γ intervals $0 \leqslant \gamma \leqslant \gamma_{max}$ which correspond to pitch angles of trapped particles.

From the results it follows that for every local minimum of B the η value varies with γ. This is in contrast to results for the standard stellarator. The sharp decrease of η marks the transition from γ corresponding to particles being trapped within one ripple well to γ corresponding to particles being trapped within a few ripple wells. For the same minimum of B the highest value of η corresponds to particles being trapped within one ripple well. Therefore, in figures for some minima of B only those η which correspond to particles being trapped within a single ripple well are shown to avoid overloading of the figures (curves 37, 57, 58, 74, 75 and 77).

For most of the minima of B, the η values are smaller than η_m for the standard stellarator ($\eta_m = 0.5$) and do not exceed 0.3 in magnitude. At the same time, there are rare minima of B for which the maximum η reaches $\eta_m \approx 0.8$ (see figure 6), which is approximately 1.6 times larger than that for the standard stellarator. However, the fraction of trapped particles of such a kind is small because the corresponding γ intervals are rather small.

In addition, one can state that the distribution of B is nearly periodic with the period length corresponding to 76 minima of B for the magnetic surface corresponding to figure 3. In this figure, the points 1 and 77, 2 and 78, etc are approximately equivalent to each other. For equivalent minimum B points the η values practically coincide (see figure 6, curves 77, 1 and 78, 2). The B distribution is also nearly symmetric with respect to point 38 (see figure 3). For those nearly symmetric minimum B points, the η values are approximately equal in magnitude but opposite in sign (see figure 4 and curves 1 and 76, 2 and 75 in figure 6). To save space, the points from 26 to 33 are not shown in figure 3 since they are nearly symmetric to the points from 50 to 43, respectively. Note that the symmetry of the B values within the examined interval is only approximate, e.g. for point 71 there is no symmetric point between points 5 and 6.

Figure 7 shows the angular distribution of points of the minima of B on the magnetic surface. The points of this scatter-plot are given for the first 76 minima of B along the magnetic field lines, which correspond to the symmetry period for the B distribution. The bold dots show the minima of B corresponding to large values of η and the straight crosses show the minima of B corresponding to small values of η. Some of these points are numbered in accordance with

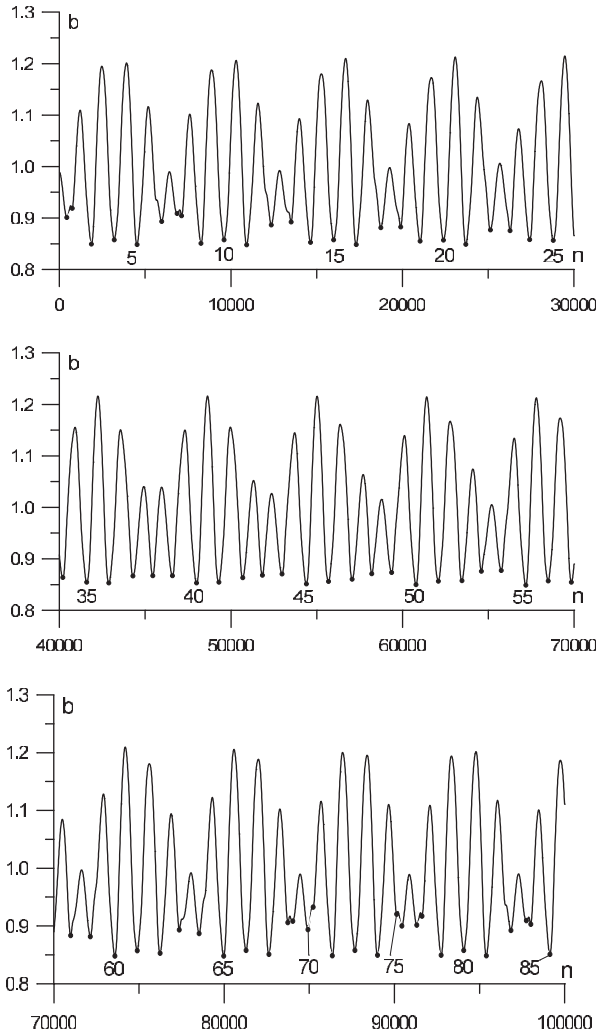

Figure 3. Distribution of $b = B/B_0$ along the magnetic field line for the outer magnetic surface (finite beta, complete data sets), n is the number of integration steps with 1280 steps per magnetic field period.

corresponding numbers of the minima of B. In accordance with the location of the $\theta = 0$ points (see figure 1), one can state that the points with the highest η values are located on the outside of the torus. The scatter-plot allows one to determine the regions on the outer magnetic surface with the highest values of local fluxes across the magnetic surface. These points corresponding to the highest values of η should be preferred as starting points for computing drift trajectories in order to find the highest values of trapped particle displacement inside the plasma.

It is interesting to note that most of the highest values of η are related to the so-called secondary minima of B along the magnetic field line (for example, points 2, 8, 68, 75, 78, etc, see figures 3, 6 and 7).

Calculations of η are also made for a magnetic surface located at a somewhat smaller plasma radius corresponding to $s = s_{32} = 0.656\,25$. For this case, the character of the obtained results is analogous to the character of the results for the outer magnetic surface.

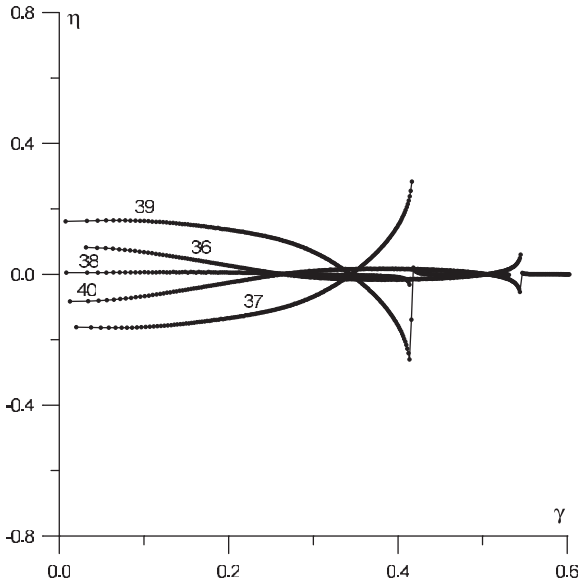

Figure 4. Parameter η as a function of γ for the outer magnetic surface in the case of finite beta and complete data sets (for local minima of B ranging from 37 to 40).

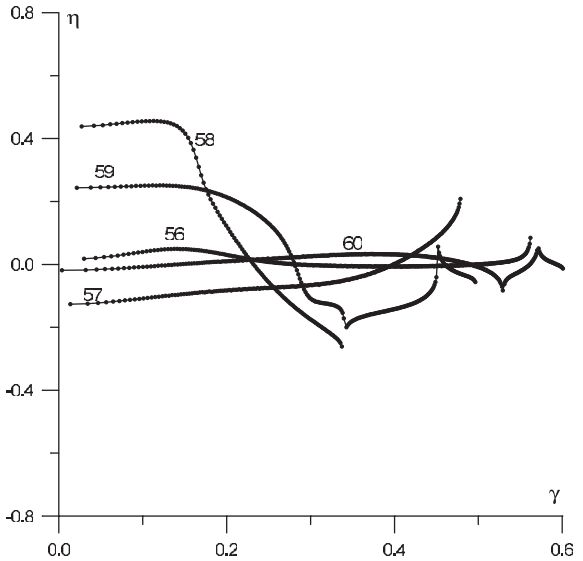

Figure 5. Same as in figure 4 for local minima of B ranging from 56 to 60.

Only the maximum values of η differ. Here, in rare cases, η only comes close to 0.38. For most of the minima of B, η_{m} does not exceed 0.25, which is about half the value for the standard stellarator model. The corresponding angular distribution of minima of B is rather close to that in figure 7.

Note that a sufficient accuracy of the η computations was confirmed in the same way as for the effective ripple computations (see the end of section 3). It is found that the maximum relative error of η does not exceed a value of 10^{-5}–10^{-6}.

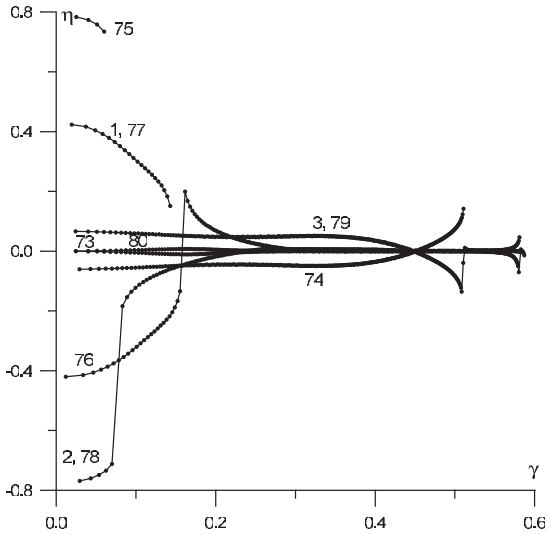

Figure 6. Same as in figure 4 for local minima of B ranging from 73 to 80 as well as 1, 2 and 3.

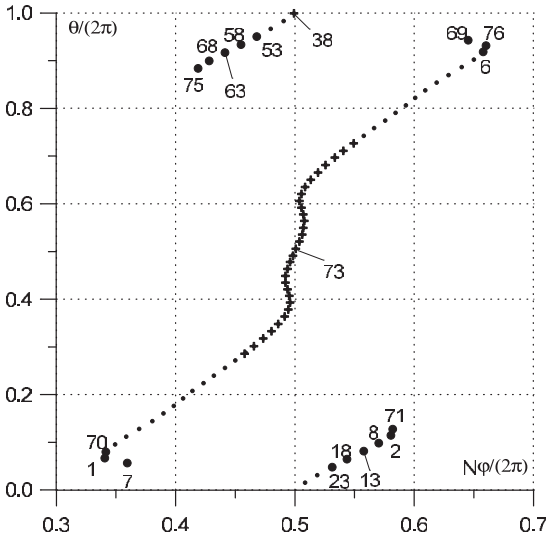

Figure 7. Angular distribution of minima of B on the outer magnetic surface for the case of finite beta and complete data sets (bold dots correspond to highest η, straight crosses correspond to small η, thin points correspond to moderate η with $|\eta| < 0.3$). For points 70, 1, 7, 23, 18, 13, 8 and 2, η equals 0.36, 0.4, 0.35, -0.3, -0.45, -0.55, -0.7 and -0.8, respectively. For the corresponding symmetric points 6, 76, 69, 53, 58, 63, 68 and 75, η values are, respectively, equal in magnitude but opposite in sign. For the point 71, $\eta = -0.8$. This point has no nearly symmetric point due to the fact that the symmetry of B is only approximate (within the examined interval).

5. Conclusion

The effective ripple for W7-X has already been studied with a Monte-Carlo technique and with the DKES code (see, e.g. [2]). A much faster code, which is based on the integration along the magnetic field lines, is used in the present paper for the evaluation of this parameter. For the finite beta case the obtained $\epsilon_{\mathrm{eff}}^{3/2}$ value of 0.001–0.0016 corresponds to the effective

ripple $\epsilon_{\rm eff}$ of 1–1.35% and correlates rather well with $\epsilon_{\rm eff}$ of 1.5% from [2]. From [2] it follows that for W7-X neoclassical transport is improved by approximately one order of magnitude with respect to W7-AS, which is not optimized with respect to the $1/\nu$ transport. Accordingly, the $1/\nu$ transport coefficients obtained in this paper are approximately ten times smaller than those for the standard stellarator. At the same time, one finds that a sufficiently large number of magnetic field harmonics is necessary to get the best converged results. The results corresponding to the ten largest harmonics (for every function) appreciably differ from those for the complete harmonic sets (825 harmonics for every function) and for the sets truncated to the hundred largest harmonics.

An analysis of the variation of the second adiabatic invariant J on magnetic surfaces is also performed in this paper for the case of finite beta using the complete data sets. From the analysis it follows that for most of the local minima of B the variation of J for W7-X is smaller than that for the standard stellarator field. This fact agrees well with the small values of the effective ripple. At the same time, for the outer magnetic surface there is a small fraction of locally trapped particles for which this variation is even greater than that for the standard stellarator. The general conclusion can be made that the orbit displacements across the magnetic surfaces for the majority of locally trapped particles are smaller, and that the fraction of trapped particles with maximum displacements is essentially less than those for the standard stellarator. The results obtained for the outer magnetic surface allow one to determine the regions on the outer magnetic surface with the highest values of local fluxes across the magnetic surface. Those points and parameters corresponding to the highest values of η should be preferred as starting points and parameters for computing drift trajectories in order to find the highest values of trapped particle displacements from the boundary surface.

For the outer magnetic surface, most of the highest values of η are related to the so-called secondary minima of B along the magnetic field line. Therefore, it is of interest to perform some changes in the Boozer spectrum of B to eliminate such secondary minima of B. Such an optimization should further improve the neoclassical transport and particle confinement in W7-X and is planned for the future.

Acknowledgments

This work was partly supported by the project INTAS-99-00592, by the Austrian Academy of Sciences and by the Association EURATOM.

References

[1] Grieger G *et al* 1991 *Plasma Physics and Controlled Nuclear Fusion Research 1990* (Vienna: International Atomic Energy Agency) vol 3, p 525
[2] Grieger G *et al* 1992 *Phys. Fluids* B **4** 2081
[3] Nührenberg J and Zille R 1986 *Phys. Lett.* A **114** 129
[4] Boozer A H 1981 *Phys. Fluids* **24** 1999
[5] Nemov V V, Kasilov S V, Kernbichler W and Heyn M F 1999 *Phys. Plasmas* **6** 4622
[6] Nemov V V 1999 *Phys. Plasmas* **6** 122
[7] Galeev A A and Sagdeev R Z 1979 *Reviews of Plasma Physics* vol 7, ed M A Leontovich (New York: Consultants Bureau) p 257
Galeev A A and Sagdeev R Z 1973 *Voprosy Teorii Plazmy* (Moscow: Atomizdat) vol 7, p 205 (in Russian)
[8] Nemov V V 1988 *Nucl. Fusion* **28** 1727
[9] Kasilov S V, Kernbichler W, Nemov V V and Heyn M F 2002 *Phys. Plasmas* **9**
[10] Beidler C D *et al* 2002 Initial results from an international collaboration on neoclassical transport in Stellarators *13th International Stellarator Workshop (25 February–1 March 2002)* (Australian National University, Canberra, Australia)